RSMAS 2004-03

Technical Report: Very-High Frequency Surface Current Measurement Along the Inshore Boundary of the Florida Current During NRL 2001

by

Jorge J. Martinez-Pedraja[1], Lynn K. Shay[1], Thomas M. Cook[1], and Brian K. Haus[2]

[1]Division of Meteorology and Physical Oceanography
[2]Applied Marine Physics Division
Rosenstiel School of Marine and Atmospheric Science
University of Miami
Miami, Florida 33149, USA

June 2004

Technical Report

Funding provided by the Naval Research Laboratory (N00173-01-1-G008) in supporting the acquisition and processing of the VHF radar measurements and Office of Naval Research Grant (N00014-02-1-0972) in the preparation of the report.

Contents

List of Tables

List of Figures

Abstract

A shore-based Ocean Surface Current Radar (OSCR) was deployed to measure ocean surface currents over the continental shelf. In support of the Naval Research Laboratory initiative, a coastal field experiment here after referred to as **NRL-2001** was conducted in the South Florida Ocean Measurement Center (SFOMC) over the narrow shelf off Fort Lauderdale, Florida in April-June 2001. The OSCR system, operating in Very High Frequency (VHF) band at 49.9 MHz, mapped surface currents vector field over a 7 km $\times$ 8 km domain with a horizontal resolution of 250 m at 700 grid points every 20 minutes. A total of 3374 samples were acquired over a 47-day period of which 81 samples (2.4%) were missing from the vector time series. An upward-looking, narrowband acoustic Doppler current profiler (ADCP) was moored in 165 m of water seaward of the shelf break sampling the current vector between 30 and 160 m at 10-min intervals.

The highly variable nature of surface currents at SFOMC responded energetically to low-frequency, wave-like meanders of the Florida Current, and the transient occurrence of multiple-scale vortices. One of the most pronounced features of the current observations during NRL-2001 experiment was a number of current reversals, some which were produced by eddies. Examination of the velocity records for the surface (OSCR) and subsurface levels (ADCP) revealed two frontal instabilities in the form of edge-eddies and two small-diameter vortices propagating through the SFOMC during the observational period. Surface currents were compared to subsurface measurements (30 m) from the ADCP, and revealed biases of 8 to 10 cm s^{-1} and slopes of O(0.4) to O(1.1) for the cross-shelf (u) and along-shelf (v) components, respectively. In the Florida Current, *rms* differences were about 18 to 34 cm s^{-1} and bulk current shears were O(10^{-2} s^{-1}) where maximum velocities exceeded 2 m s^{-1} at the surface and 1.4 m s^{-1} between 30 and 50 m. Tidal currents were masked by the fluctuations of the Florida Current, but only explained about 1% of the observed current variance.

Acknowledgments

The authors gratefully acknowledge funding provided by the Naval Research Laboratory (N00173-01-1-G008) in supporting the acquisition and processing of the VHF radar measurements and Office of the Naval Research Grant (N00014-02-1-0972) in the preparation of the report. We would also like to thank Mr. Jose Vasquez of the City of Hollywood Beach and Mr. Jim Davis of Broward County Parks and Recreation for supporting our operations. Ms. June Carpenter allowed us access to her beach house for OSCR operations. Dr. Renate Skinner and Mr. Sid Leve permitted us to use the beach at the John U. Lloyd State Park. The research was conducted under the auspices of the South Florida Ocean Measurement Center. We also thank Dr. William Venezia for the ADCP current measurements at the U.S. Navy Test Facility.

1 Introduction

Currents over the inner shelf are highly variable and respond to forcing at different temporal and spatial scales by winds, tides, internal waves, topographic modulations, as well as intrusions of ocean fronts depending on the venue. However, along the narrow continental shelf off Fort Lauderdale, ocean currents tend to be driven by the Florida Current (FC) and the cyclonic shear vorticity along the inshore edge of the current. Areas of frontal zones, especially when as clearly expressed as the edge of the FC, are typified by considerable dynamic instability. Modulations of the inshore FC front are revealed in the form of either horizontal wave-like meanders or the passage of submesoscale eddies with strong horizontal shear (Lee, 1975; Shay *et al.*, 1998).

To capture the transient events from single-point measurements such as moorings or drifters is very difficult. For these reasons, a land-based high frequency (HF) Doppler radar system was employed to investigate coastal sea-surface processes. In this framework, HF-radar measurements provide both the spatial and temporal resolution required to observe these processes. The first HF-radar system for mapping ocean surface currents was used over 30 years ago (Stewart and Joy, 1974; Barrick *et al.*, 1974). The use of HF-radar technique continues to increase in coastal oceanographic experiments (Prandle, 1987; Haus *et al.*, 1998; Shay *et al.*, 1995, 2002, 2003).

HF-radar technique provides a unique means to measure surface currents by transmitting radar signals over the sea surface and analyzing the Doppler frequency spectrum of the backscattered echoes. This scattering mechanism by which the surface current can be obtained from the spectrum is known as Bragg resonance (Stewart and Joy, 1974). The Ocean Surface Current Radar (OSCR) system utilizes an 85 meter, 16 (HF) or 32 (VHF) element phased-array antennae to achieve a narrow beam, electronically steered over the illuminated ocean area. The beamwidth is a function of the radar wavelength divided by the length of the phased array, which is 7° for the HF mode and 3.5° for VHF mode, respectively. Theoretical and observed beam patterns were compared for a 16-element phased array in a comprehensive review of the HF-radar issues by Gurgel *et al.* (1999), who found that the surface current measurements from a phased array were well-resolved.

Evaluations of ocean surface currents from HF Doppler radars have been made by comparing subsurface currents measurements from both fixed and moving platforms during a series of experiments. Expected differences depend on instrument measurement error, sampling characteristics and geophysical variability associated with Stokes drift, Ekman drift, and baroclinicity (Graber *et al.*, 1997), as well as tidal currents and internal waves (Shay, 1997). More recently a comparison between surface currents derived from the VHF (49.9 MHz) mode of OSCR and subsurface currents 3 to 4 m beneath the surface from moored and ship-board ADCP acquired during the summer of 1999 in the South Florida Ocean Measurement Center (SFOMC) indicated regression slopes of O(1) with biases ranging from 4 to 8 cm s^{-1} (Shay *et al.*, 2002). In the following report, VHF-radar current measurements acquired in 2001 during NRL experiment in the SFOMC are described.

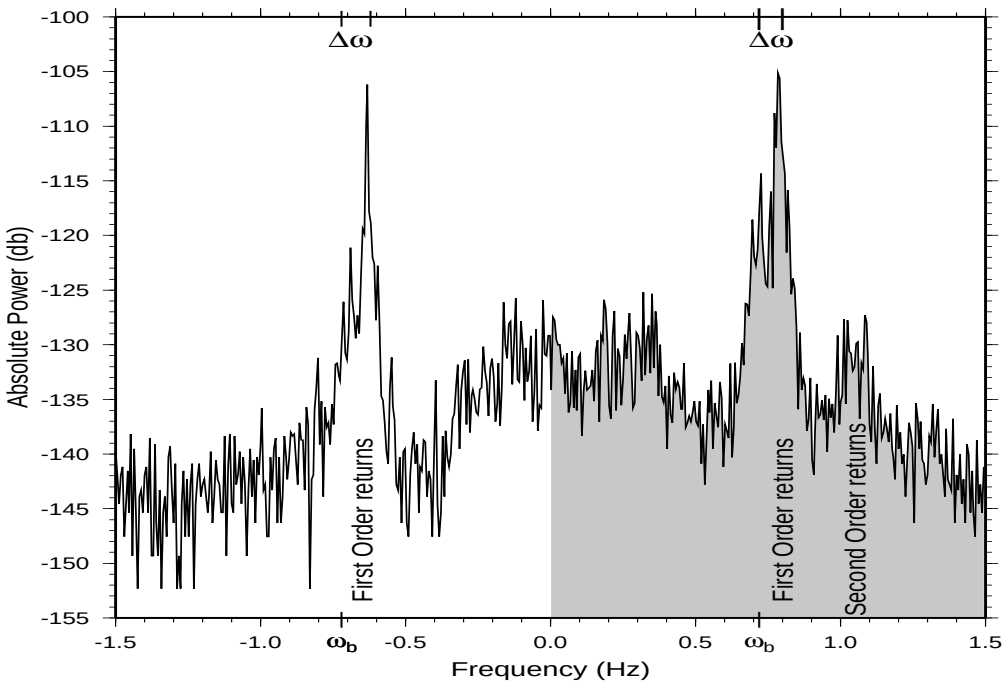

Figure 1: Doppler spectrum as observed by OSCR showing the Doppler-shifted peaks away from the theoretical position of the radar Bragg peaks depicted by ω_b (≈ 0.712 Hz) for VHF radar.

2 Experimental Design

2.1 HF Doppler Radar

The Doppler radar technique was originally described by Crombie (1955), who observed that the echo Doppler spectrum consisted of distinct peaks, symmetrically positioned about the Bragg frequency (Figure 1). The concept is based on the premise that pulses of electromagnetic radiation are backscattered from the moving ocean surface by resonant surface waves at one-half of the radar wavelength or "Bragg waves". The wavelength, λ_B, of the Bragg waves is given by

$$\lambda_B = \frac{\lambda_r}{2\sin\theta_i}, \tag{1}$$

where λ_r is the radar wavelength and θ_i is the incidence angle. For the HF radar system, $\theta_i = 90°$, so λ_B for this case is equal to one-half the radar wavelength. The Bragg scattering effects results in two discrete peaks in the Doppler spectrum. In the absence of a surface current, the position of these spectral peaks is symmetric and their frequency, ω_B, is given by

$$\omega_B = \frac{2C_o}{\lambda_r}, \tag{2}$$

where $C_\circ = \sqrt{(g/k_B)}$ is the linear phase speed of the surface Bragg wave in deep water. The two peaks resulting from Bragg resonant scattering (constructive interference) originate from two targets traveling at constant velocity on the ocean surface, one advancing and the other receding from the radar array (Stewart and Joy, 1974).

If there is an underlying surface current, Bragg peaks in the Doppler spectrum are displaced from ω_B by an amount

$$\Delta\omega = \frac{2V_r}{\lambda_r} \tag{3}$$

where V_r is the radial component of surface current along the radar look-direction. The surface vector current is computed by combining two radial components emanating from the two stations. Velocity components parallel and normal to the two intersecting radials are expressed in terms of the radial velocity components

$$V_p = \frac{R_m + R_s}{2\cos(\Delta/2)}, \tag{4}$$

$$V_n = \frac{R_m - R_s}{2\sin(\Delta/2)}, \tag{5}$$

where,

$$\Delta = \theta_s - \theta_m, \tag{6}$$

and R_m and R_s are the radial velocity components and θ_m and θ_s are the bearings of the radials emanating from master and slave sites, respectively. The east and north components corresponding to the velocity vector U are expressed as

$$u = V_p \sin\alpha + V_n \cos\alpha, \tag{7}$$

$$v = V_p \cos\alpha - V_n \sin\alpha, \tag{8}$$

where

$$\alpha = \frac{\theta_s + \theta_m}{2} \tag{9}$$

is the average angle of the radial bearings rotated clockwise with respect to the true north. Substitution of (4) and (5) into (7) and (8) yields

$$u = \frac{R_s \cos\theta_m - R_m \cos\theta_s}{\sin\Delta}, \tag{10}$$

$$v = \frac{R_m \sin\theta_s - R_s \sin\theta_m}{\sin\Delta}, \tag{11}$$

Note that measurement errors increase if the angle between the radar pulses becomes small in the far-field. For angles, (Δ), less than 30° and greater than 150° generally no vector currents are computed. However, under certain circumstances (e.g., the current is aligned along the radials), this envelope can sometimes be relaxed and reduced by ∼15°. This geometric criterion is used to eliminate measurements at sharp and shallow angles between two radials.

2.2 Ocean Surface Current Radar (OSCR)

The University of Miami Ocean Surface Current Radar (OSCR) system utilizes either HF (25.4 MHz) or VHF (49.9 MHz) radio frequencies to map surface current patterns over a large area in coastal waters. The shore-based radar system consists of two units (master and slave) which are deployed 4 to 30 kilometers apart. Effective ranges of the HF and VHF modes of this

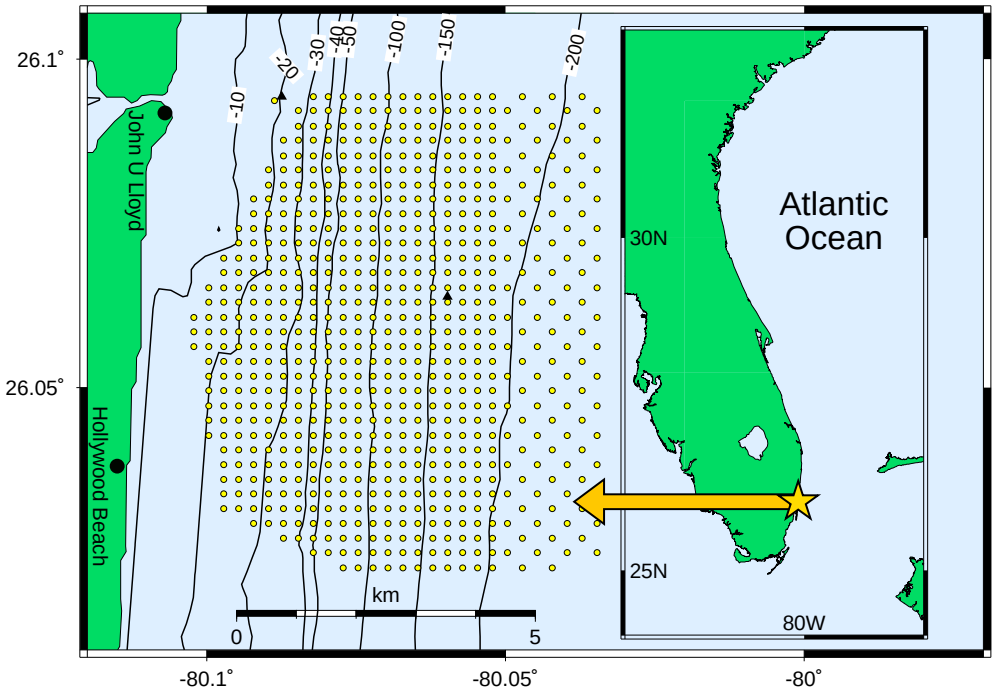

Figure 2: OSCR cell locations for NRL-2001 experiment and bottom-mounted ADCP mooring sites (triangles).

pulsed radar differ significantly. For example, the pulse repetition intervals (T_{rep}) are 310 μs and 80 μs for the HF and VHF (see Table 1) modes, respectively. The duration for pulses (T_{dur}) in each mode are 13.3333 μs and 1.667 μs, and the estimated effective range is given by

$$R = \frac{c}{2}(T_{rep} - T_{dur}), \tag{12}$$

where c is the speed of light (2.9998×10^8 m s^{-1}). For the HF mode, the theoretical range is 44 km whereas in VHF mode it is 11 km. These effective ranges are also important for the baseline separation distances between the two stations (3 to 7 km for VHF mode and 20 to 30 km depending upon configuration for HF mode) (Shay *et al.*, 2002). The receive antenna system consists of a phased-array that uses beamforming and range-gating to measure the Doppler spectra from 700 different cells from backscattered signals. In the VHF operational mode, these cells have a nominal area of ≈ 0.06 km^2.

Master and slave units acquire independent current measurements along radial beams containing the reflected signals received by its phased-array antennae system. The measurement interval between each vector current map is 20 minutes as radar data are acquired from the master over a 5-minute period, followed by a similar time period by the slave system. Returns are processed by FFT analysis to give the Doppler spectra at each cell. Radial currents are subsequently extracted

Parameter	HF	VHF
Frequency (MHz)	25.4	49.9
Range (Km)	44	11
Range Resolution (Km)	1	0.25
Azimuth Resolution (^{o})	8 - 11	4 - 5.5
Measurement Cycle (min)	20	20
Spatial Coverage (km^2)	700	70
Max. number of measurement points	700	700
Measurement Depth (m)	0.4	0.2
Data Storage (days)	120+	120+
Transmitter Peak Power (KW)	1	0.1
Transmitter Average Power (maximum) (W)	21	10
Power Consumption (KW 240V)	<1	<1
Transmit Antennae Elements (Yagi; 6dB gain)	4	4
Recieve Antennae Elements (phased array)	16	32
UHF communication (MHz)	458	458
Transmit Time (s)	293.6	293.6
Pulse length (μs)	13.333	1.667
Pulse repetition interval (μs)	310	80
Accuracy		
Radial Current (cm s^{-1})	2	2
Vector Current (nominal) (cm s^{-1})	4	4
Vector direction (^{o})	5	5

Table 1: OSCR system capabilities and specifications.

from the spectra and then combined, to form the two-dimensional vector currents (speed and direction) based on range and bearing to each of the 700 cells. The measurements can be made simultaneously at these cells either at 1 km (HF mode) or 250 m (VHF mode) nominal resolution. Specifications and capabilities of the OSCR system are listed in Table 1.

2.3 Site Location and Measurement Domain

To measure the vector currents, the OSCR system requires two independent, but linked stations with overlapping field of view over a coastal ocean or estuary. The OSCR receiving antenna array is installed as close to the sea as possible to improve the conductivity of the ground plane and the coupling to the sea (Kingsley *et al.*, 1997). The OSCR transmitting antenna is located as near to the sea as possible to minimize propagation losses over land. Suitable ocean front locations are limited by the requirement for a relatively long ($\sim$ 90 m) area of open and unobstructed beach from which to illuminate the measurement domain. The spacing between the two stations influences the areal coverage for vector current sampling and must be carefully chosen to optimize the desired experimental domain and the sampling of dominant flow patterns.

During the NRL experiment, the OSCR radar system overlooked a portion of the SFOMC range, starting on 28 April and ending 14 June 2001. During this period, a 47-d continuous

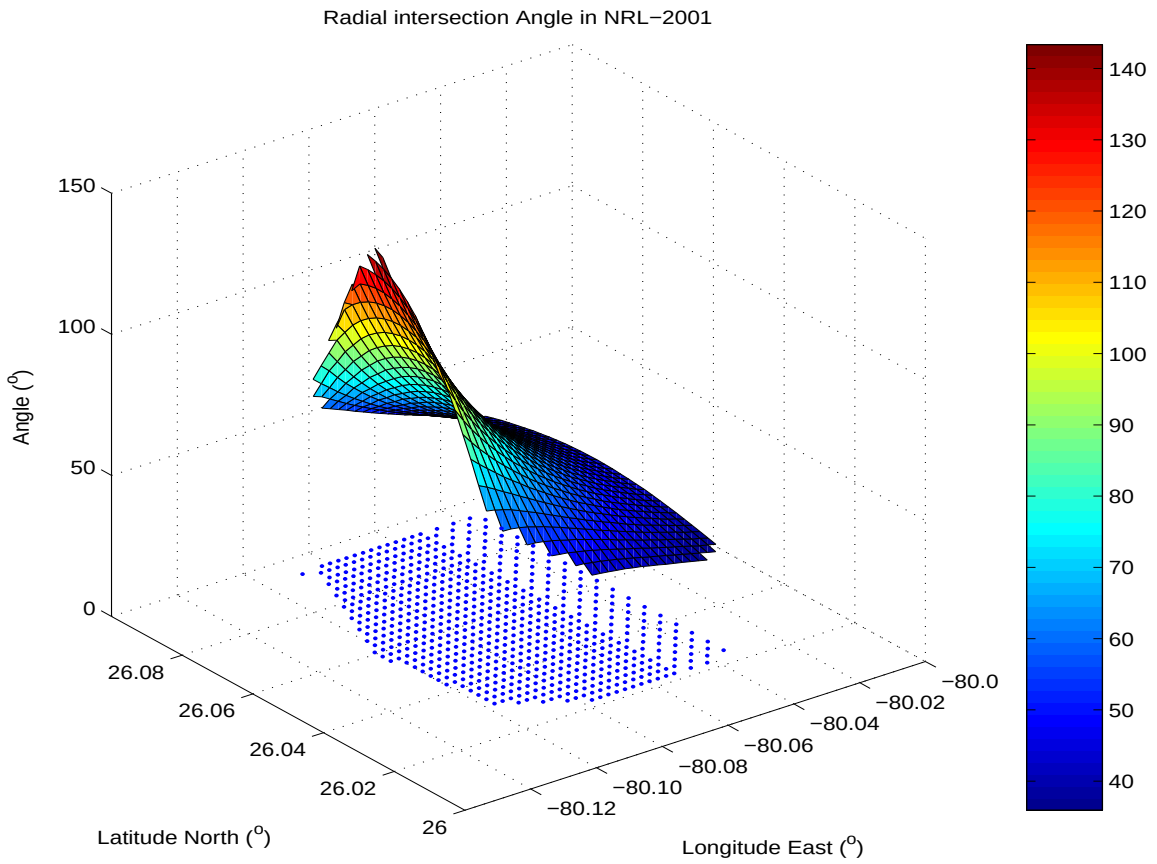

Figure 3: Angle of intersection of the radial beams for the NRL-2001 configuration.

time series of vector surface currents was acquired at 20-min intervals. The system was used in VHF mode and sensed the electromagnetic signals scattered from surface gravity waves with wavelengths of 2.95 m. Radar sites were located in John U. Lloyd State Park (adjacent to the US Navy Surface Weapons Center Facility) (Master) and an oceanfront site in Hollywood Beach, FL (Slave), equating to a baseline distance of approximately 6 km. Each site consisted of a four-element transmit and thirty-element receiving array (spaced 2.95 m apart) oriented at an angle of 37° (SW-NE at Master) and 160° (SE-NW at Slave). The VHF radar system mapped coastal ocean currents over a 7 km × 8 km domain with a horizontal resolution of 250 m at 700 grid points in the SFOMC (see Fig. 2). The position of the bottom-mounted ADCP mooring operated by the U.S. Navy is shown as a triangle in 160 m of water.

2.4 Measurement Resolution

The geometric coverage of the radar is constrained by the physical orientation and placement of the receive antenna arrays. The acceptable angle between two radials beams must fall between $30° \leq \triangle \leq 150°$ for reliable measurement of vector currents as noted above, and the maximum effective range for the present OSCR configuration is limited to 11 km. These angles are also fixed for a particular experiment, with the optimum value of $\triangle \sim 90°$ and the minimum value for which reasonable vector currents can be computed (35° for NRL-2001), shown in Figure 3 are the

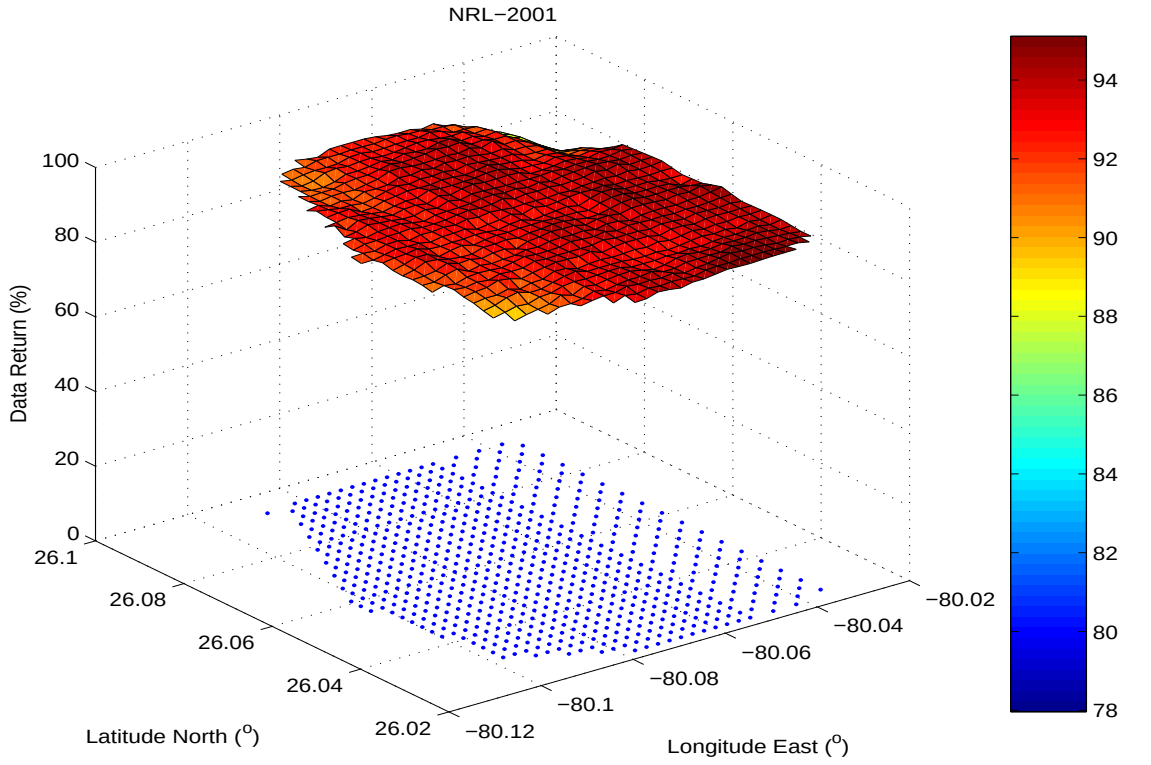

Figure 4: Percent of data return during the NRL-2001.

angles for each of the OSCR cells. It reveals the angle of intersection of the radials is appropiate for the 700 cells. Hence, reasonable vector currents were computed. The resolution of the radial velocities of OSCR system is related to the dwell time of the radar. The uncertainty introduced by determining the vector velocity in this manner depends upon the resolution of each radial measurement, the angle between the radials and the direction of the measured current (Chapman *et al.*, 1997; Graber *et al.*, 1997). The manufacturer states accuracies of the radial, and vector speed of 2 and 4 cm s^{-1} respectively with a directional resolution being 5° (Table 1). The accuracy of OSCR measurements has been examined by Chapman *et al.* (1997), Haus *et al.* (2000), and Shay *et al.* (1995, 1998b, 2002, 2003). These studies demonstrate that the remote sensing of surface currents in coastal areas using phased array radars is an accurate technology suitable for wider use within the oceanographic community.

3 Data Return and Quality

During the NRL experiment, a total of 3374 samples were acquired from 16:40 GMT 28 April to 13:00 GMT 14 June 2001, yielding a 47-d time series. Of the 3374 samples, only 81 were missing from the vector current time series, equating to 2.4% loss in the samples. The percentage of the total 3374 samples that could be acquired at each cell is shown in Figure 4. For the entire range of 700 cells, the data return exceeded 92%. These experimental results using the VHF mode are the highest with respect to overall data return relative to previous experiments using OSCR

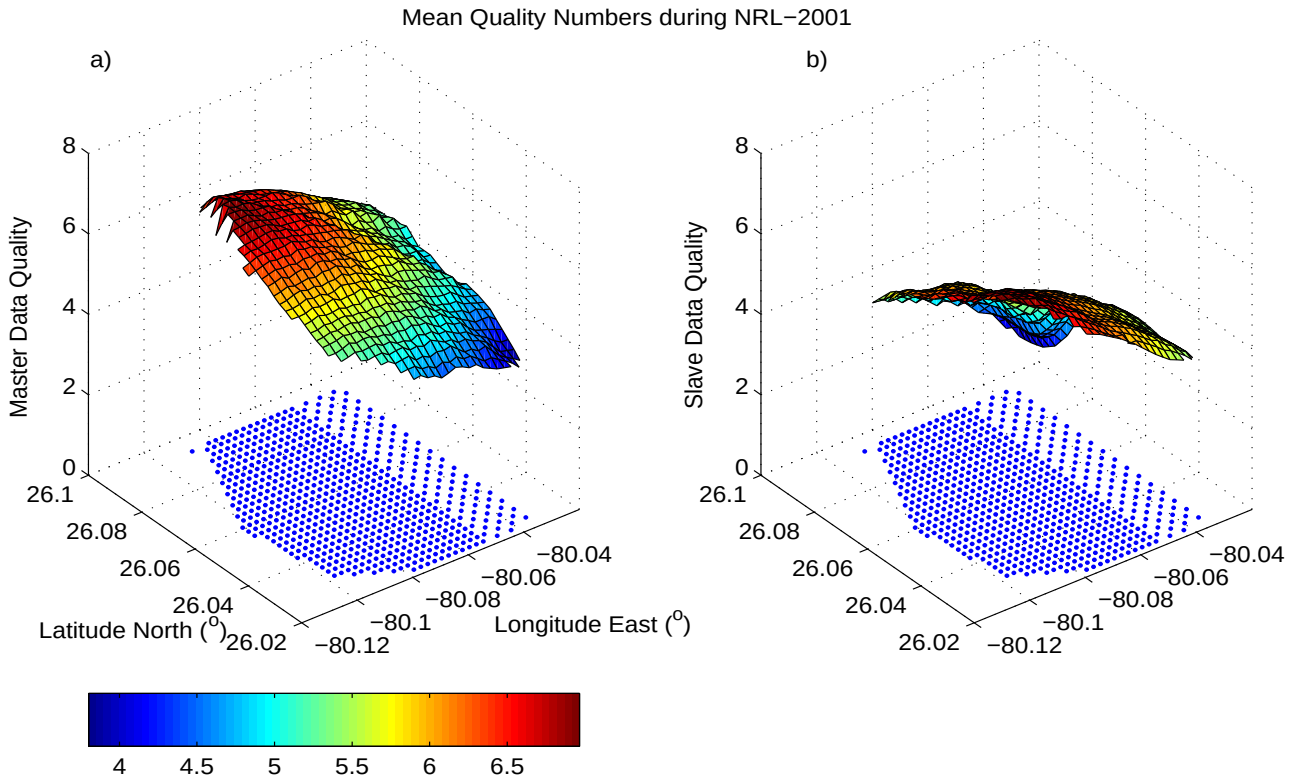

Figure 5: Mean (a) Master (left) and (b) Slave (right) quality numbers from the NRL-2001 experiment.

in both modes.

One of the main measures of the quality of the return signal in the collected data is the Bragg line quality, which is a classification of how well the dominant Bragg peaks are resolved in the Doppler spectra. The simplest criterion looks at how many Bragg peaks are present in the spectral record. Under typical conditions, two peaks occur and are preferred for deriving radial currents. The greater the peaks are above the noise level and narrower the Bragg separation, the more robust and accurate is the computation of the radial currents resulting in a higher quality number. Single peak spectra have lower quality numbers, because the current velocity estimate along the beam depends on additional parameters such as water depth, water density and salinity. Doppler spectra which exhibit no peak above the noise level are considered of **zero** quality. The overall average quality numbers for the Master and Slave spectral data during NRL-2001 are shown in Figures 5a and 5b respectively. Figure 6 shows the quality numbers of all Doppler spectra measured at the two stations. The distributions of the quality numbers are similar for both stations. More than 80% of the Doppler spectra at both stations display two Bragg peaks corresponding to waves either approaching or receding from the radar stations.

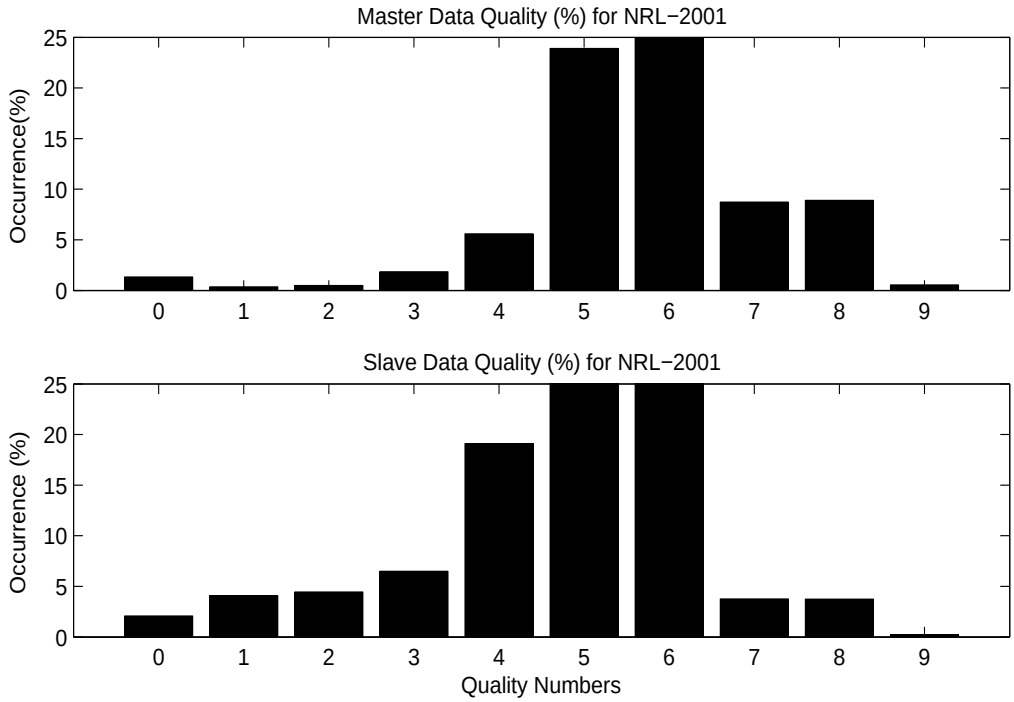

Figure 6: Histograms of quality numbers of the Doppler spectra measured at the Master (upper panel) and Slave (lower panel) OSCR stations.

4 Observations

4.1 Atmospheric Conditions

Near-surface wind and pressure records from a Coastal Marine Automated Network (CMAN) station at Fowey Rocks (25°35.4'N, 80°6.'W) indicated that atmospheric conditions during the experiment were relatively calm with a mean wind speed of 6.6 m s^{-1}. During the first 16 days, winds between 3 to 9 m s^{-1} were predominantly onshore, directed towards south-west (Figure 7). The wind direction subsequently reversed to northerly and followed that direction with some fluctuations from mid May through June. Surface pressures fluctuated between 1013 to 1020 mb during the observational period. Observed surface meteorological conditions were similar to those observed at Lake Worth CMAN station (not shown).

4.2 Surface Current Observations

Surface flows are highly variable in the regime off the SFOMC where wind-driven flows dominate the near-shore region. However, surface flows across the outer shelf are controlled by the FC. Observed surface currents in the region of SFOMC were complex and exhibited significant spatial and temporal variability with frequent intrusions of the FC over the shelf break in the form of either horizontal wave-like structures along the inshore edge of the current, or multiple-scale vortices. Accounting for a deformation radius of the order of 10 km for this regime (Shay *et al.*, 2000), submesoscale and mesoscale features were observed just inshore of the FC in a high

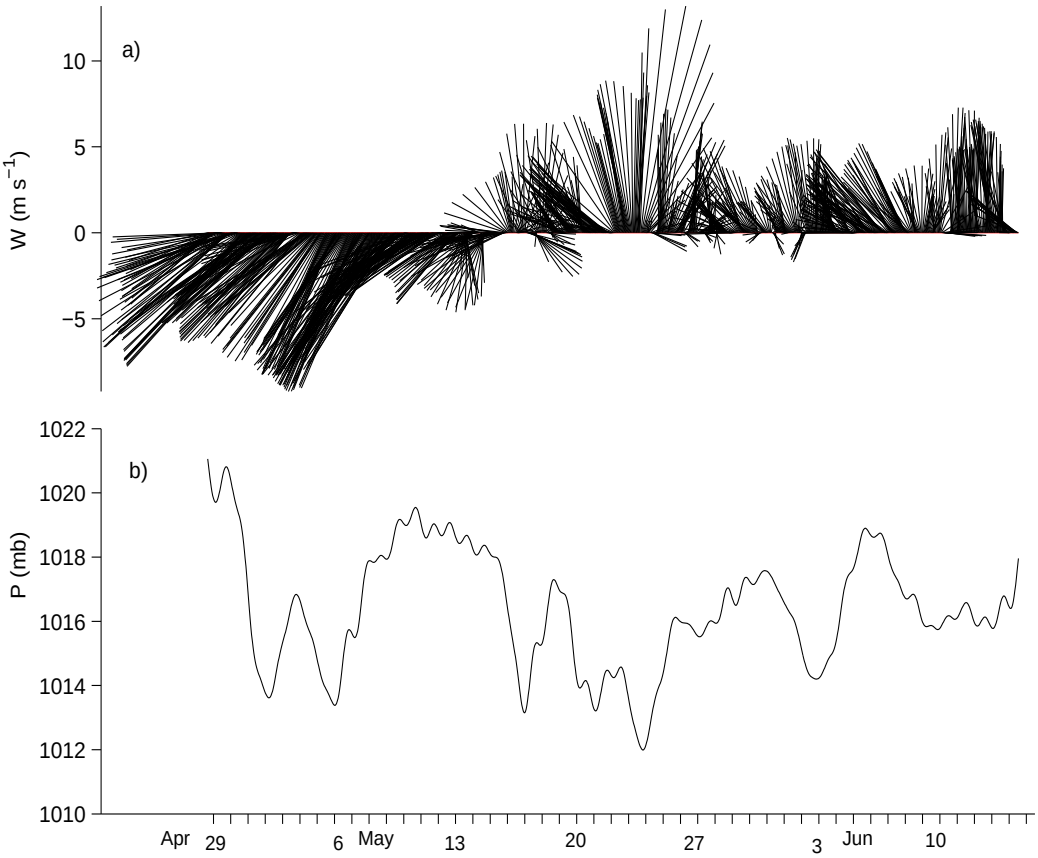

Figure 7: (*a*) Surface wind (m s^{-1}) and (*b*) surface pressure (mb) from hourly observations at the CMAN station at Fowey Rocks located south of the VHF radar domain in April-June 2001. Surface wind was placed into an oceanographic context.

horizontal current shear zone (Peters *et al.*, 2002).

On 1 May, a cyclonically rotating eddy-like feature was detected along the inshore edge of the FC (Figure 8), when along- and cross-shelf scales exceeded 8 km. Maximum surface currents were 40 to 50 cm s^{-1} in the domain. The FC penetrated onto the shelf over the next 48 hours, moving farther offshore over the next 13 days as relatively weak and fluctuating currents dominated the SFOMC region. On 18 May, a submesoscale vortex entered into the region (Figure 9) with a radius of $\sim$ 3 km and a northward along-shelf advection velocity of $\sim$ 60 cm s^{-1}. The center of rotation located $\sim$ 4 km from the coastline with nearshore currents of 20 to 40 cm s^{-1} and offshore currents between 50 to 100 cm s^{-1}. Four days later (22 May), a marked current reversal occurred along the inshore region of the FC toward the south with a cyclonic rotation (Figure 10), that did not appear to be either tidally driven or wind induced. One possibility is that this eddy-like feature had characteristics consistent with the large-scale spin-off eddies described by Lee (1975) and Lee and Mayer (1977). This feature advected northward with a horizontal scale that could not be resolved by the measurements in the high-resolution VHF domain. On 1 June, another vortex moved into the region (Figure 11). This feature propagated northward at a mean speed of about 65 cm s^{-1} with a radius of $\sim$ 1.3 km. Along the inshore edge, surface currents were directed toward the south at 20 to 50 cm s^{-1} with offshore current of 50 to 100 cm s^{-1}. Other weaker current reversals of FC occurred during this experiment, but were not necessarily

produced by eddies or small-scale vortices. In addition, low-frequency current fluctuations of the FC in the form of wave-like meanders, with time scales ranging from 2 to 13 days, were detected during the observational period. These features with similar periods, were observed before by Parr (1937), Lee (1975) and Lee and Mayer (1977).

These modulations of the inshore front of the FC in the form of either horizontal wave-like meanders or the passage of multiple-scale vortices induced current variations in the region with significant cross-frontal shear of the along-shelf velocity along the shelf break (Figure 12). Offshore meanders of the FC often displace the high frontal shear region farther offshore. In these cyclonic shear zones, Peters *et al.* (2002) noted the ambient vorticity of 4 to 5 f (where f the local Coriolis parameter) in the northward flow of the FC. That is, the normalized vorticity can be used as a proxy for the Rossby number, suggesting that this regime is highly nonlinear.

Along-shelf surface currents ranged from 40 to 150 cm s^{-1} when the FC moved shoreward, with a weak cross-shelf component (less than 10 cm s^{-1}). Mean and standard deviations of the surface currents were estimated from the 47-d time series. Beyond the shelf break, surface currents exceeded 50 cm s^{-1} (Figure 13a) consistent with the close proximity of the FC to the coast. Inside the shelf break, mean currents ranged between 10 to 30 cm s^{-1}. The region beyond the shelf break had the highest standard deviation (Figure 13b), and hence surface current variability, which was the result of the FC fluctuations, winds and tides.

4.3 ADCP Mooring Measurements

During the NRL-2001 experiment, a bottom-mounted, upward-looking RDI 300 kHz ADCP was deployed in the central portion of the HF-radar domain at 165-m depth in the SFOMC (Table 2). This profiler sampled the current structure at 10 min intervals over 4-m vertical bins for a total of 40 bins starting approximately 5-m above the bottom for the mooring and extending to within 2-m of the surface. The first 7 bins (2-26 m) from the surface were not considered because the data were not usable due to sidelobe contamination. As shown in Figure 14, several FC intrusions were observed during the experiment. During these episodes, upper ocean current velocities exceeded 150 cm s^{-1}. The current structure between surface to 70 m depth followed similar trends, showing vertical coherence and suggesting that the FC contains both depth-independent (i.e. barotropic) and depth-dependent (i.e. baroclinic) velocities (Shay *et al.*, 1998, 2002).

Instrument	Lat (°N)	Long (°W)	Water Depth (m)	Sensor Depth (m)	Sampling Interval(min)
OSCR (Cell 473)	26° 3.78'	-80° 3.58'	165	surface	20
ADCP (NSWC-A)	26° 3.83'	-80° 3.58'	165	2-163	10

Table 2: Instrument types and locations during NRL-2001 experiment.

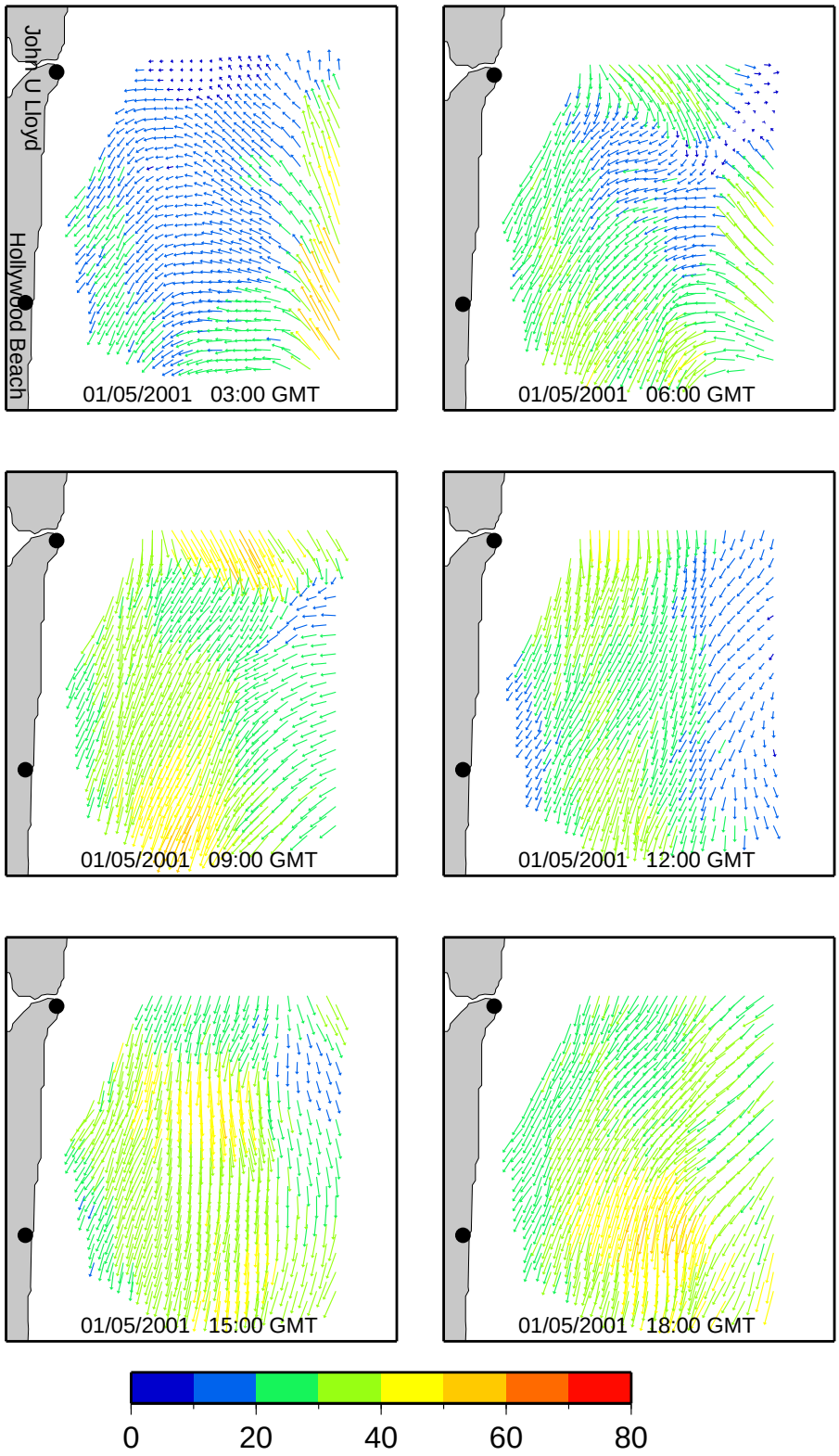

Figure 8: Surface current imagery of 1 May 2001 where the color of the current vectors depicts magnitude of the current as per the color bar in cm s^{-1}.

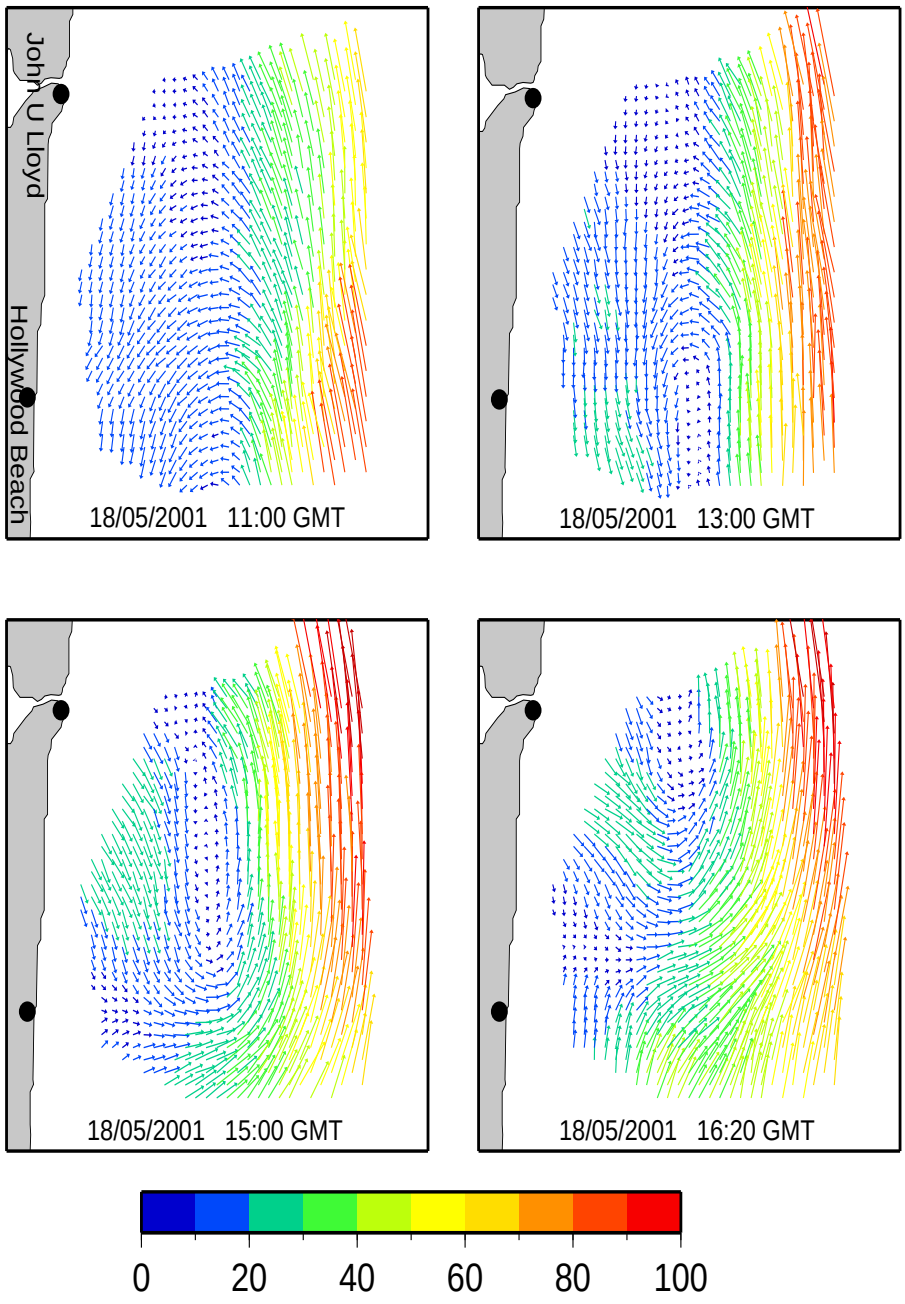

Figure 9: Same as Figure 8 except for 18 May 2001.

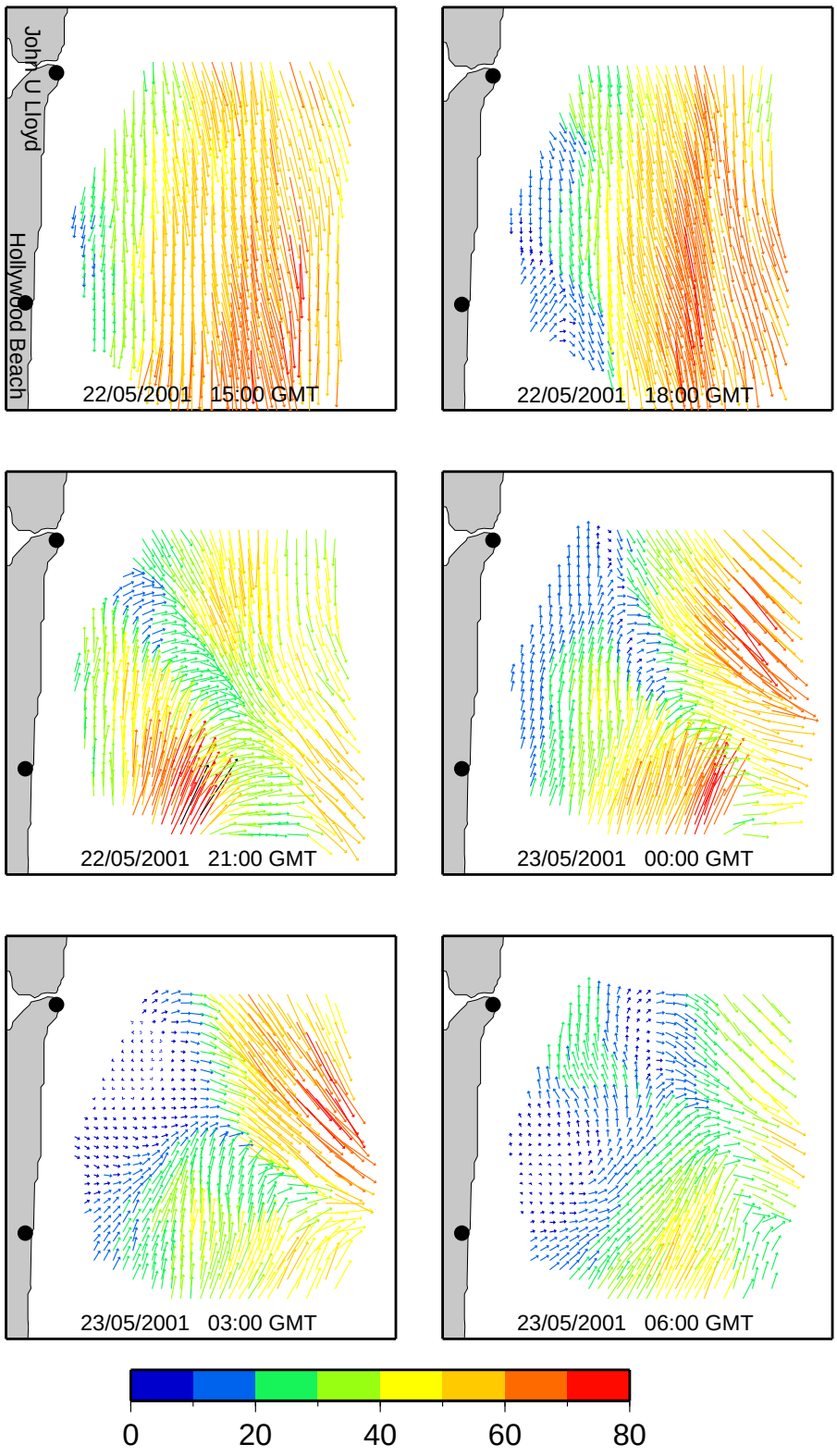

Figure 10: Same as Figure 8 except from 22-23 May 2001.

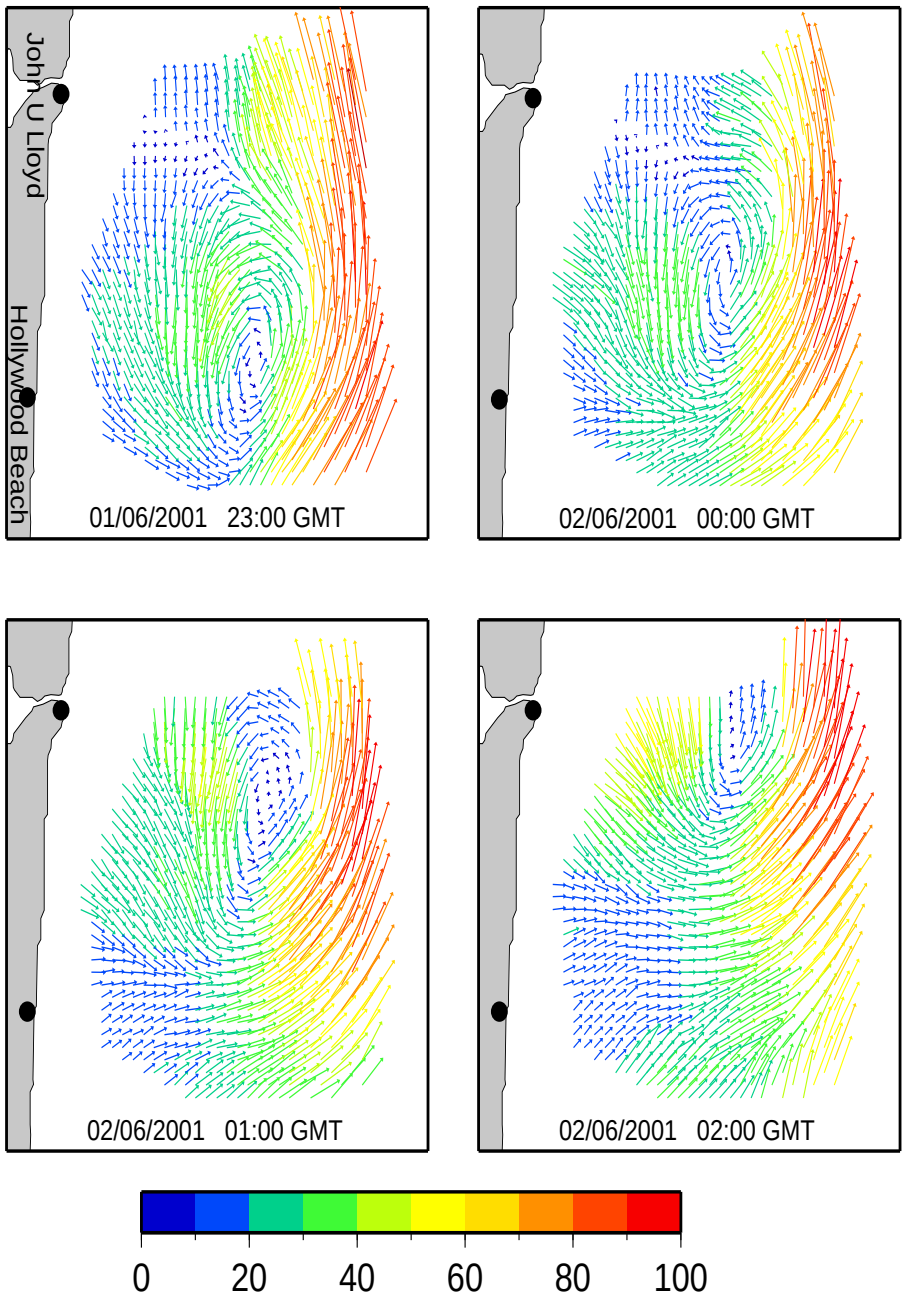

Figure 11: Same as Figure 8 except from 2 June 2001.

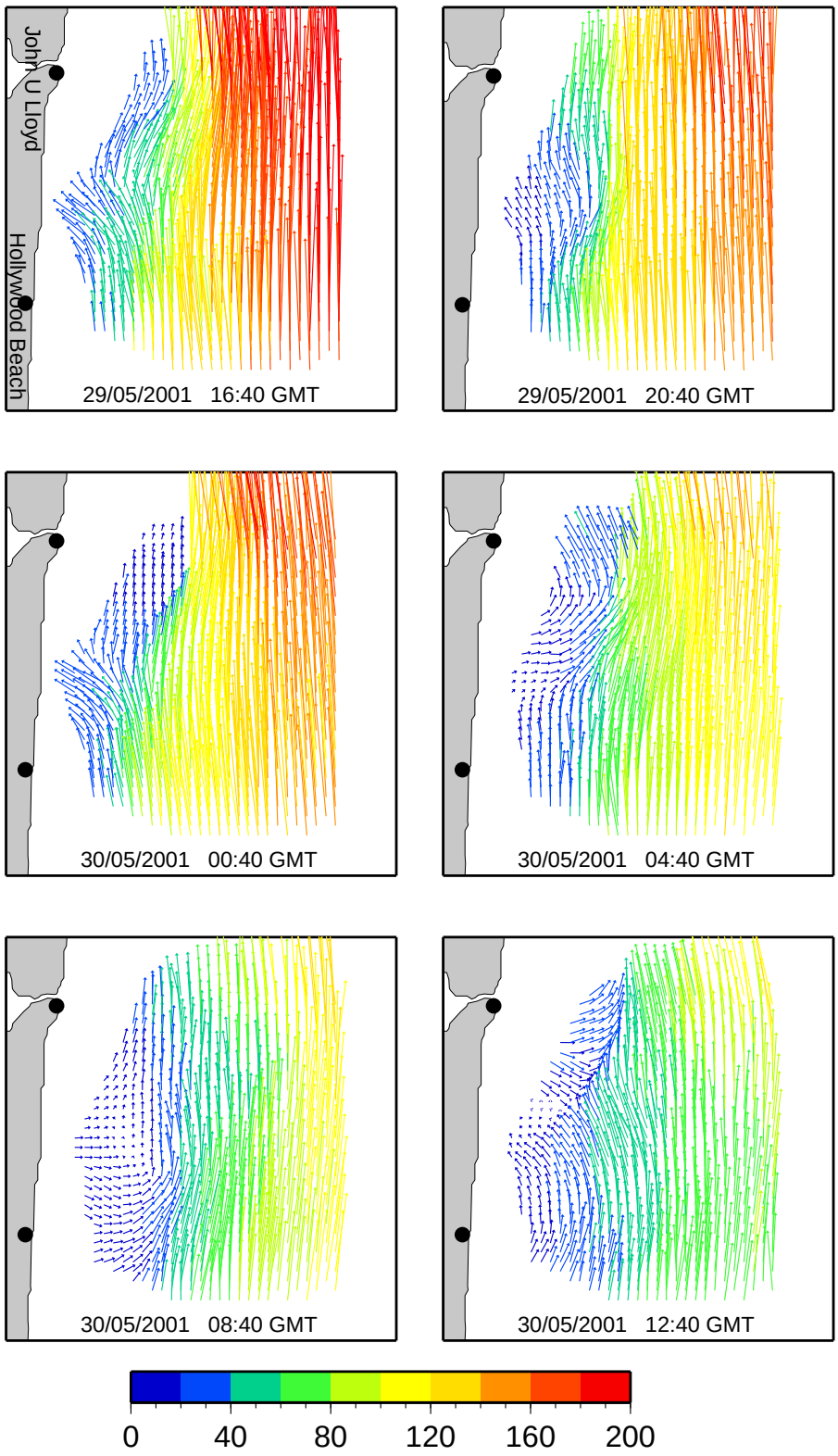

Figure 12: Same as Figure 8 except for 29-30 May 2001.

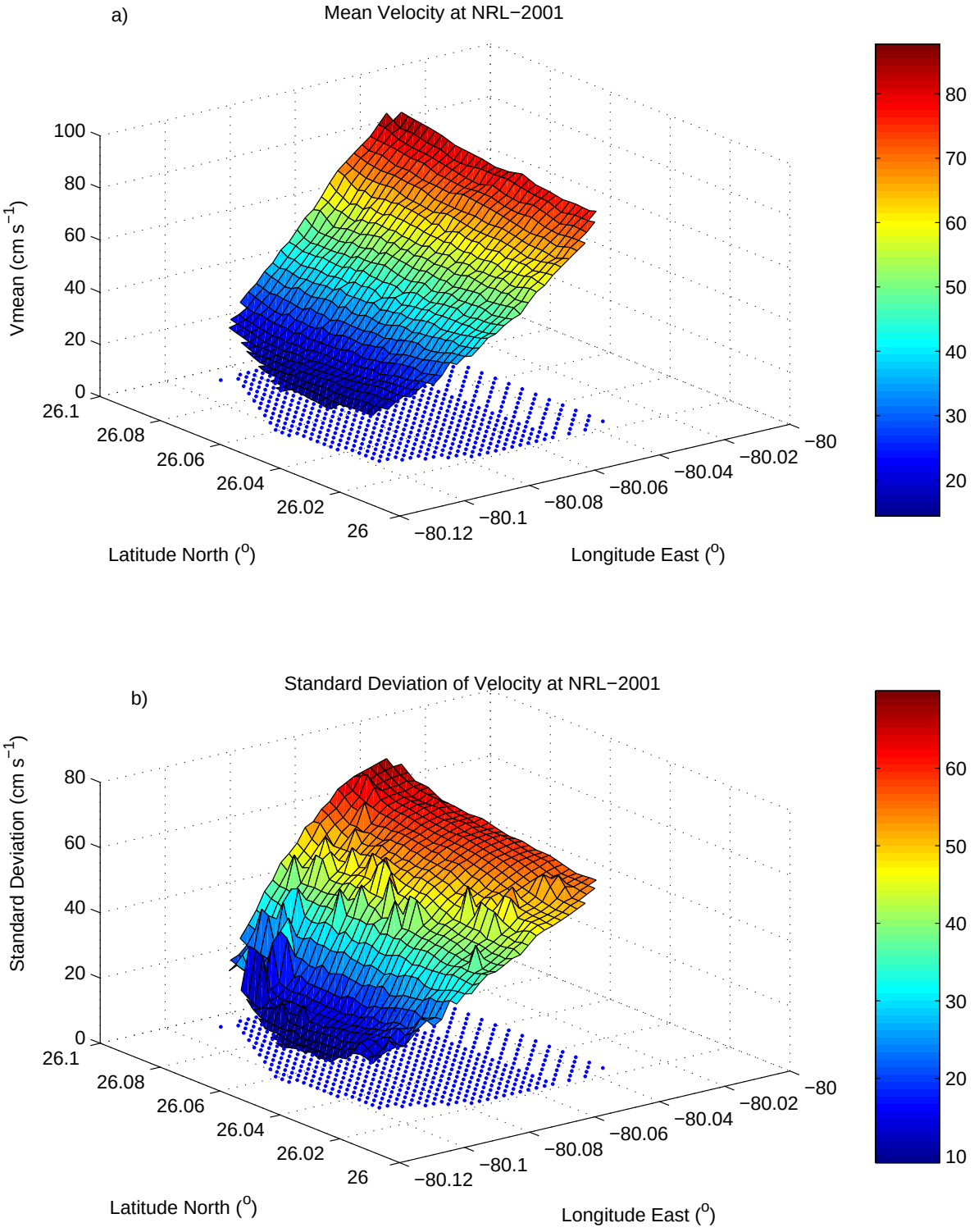

Figure 13: (*a*) Mean surface velocities, (*b*) standard deviation of surface velocities.

Initially, currents throughout the column indicated an along-shelf flow of 50 to 120 cm s^{-1} toward the north. On 1 May, the current structure reversed to a southward along-shelf flow, suggestive of a spin-off eddy confined to the upper 60-m in the water column (Shay, 1997), and over the next day, a FC intrusion forced an along-shelf flow toward the north with current velocities of ∼50 cm s^{-1}. As the FC moved farther offshore, weak oscillatory currents between 5 to 20 cm s^{-1} were observed above 70-m depth over the next two weeks, whereas the current was towards the south below 90-m. A FC reversal throughout the entire water column was evident on 22 May, which was presumably caused by the passage of a frontal instability induced by a spin-off eddy. After this reversal, a strong FC intrusion was observed with a predominant northward along-shelf flow ranging between 50 to 150 cm s^{-1} with larger upper ocean currents. RMS differences between adjacent ADCP bins were examined from 30 to 150 m depth (not shown) to understand observed subsurface current variability. For the cross-shelf currents, this variability ranged between 2 to 10 cm s^{-1} throughout the water column. However, a significant difference of 47 cm s^{-1} was found between 70 to 90 m depth for the along-shelf currents, mainly due to the excursion of the FC farther offshore (mentioned above) from 4 to 16 May. In the upper 70 m, the current variability ranged between 3 to 7 cm s^{-1}, below 90 m observed differences were 6 to 15 cm s^{-1}. This variability is relevant to the comparisons with the surface currents discussed below.

4.4 Data Comparisons

To evaluate the radar-derived surface current measurements, vector currents at cell 473 were compared to the ADCP current profile (Table 3) over the 47-d time series. Averaged surface current vectors were estimated with a spatial resolution of 250 m in the top 0.2 m of the water column. To facilitate direct comparisons between the surface and subsurface velocities, ADCP data were smoothed using a 3-point Hanning window and subsampled at 20-minute intervals.

Moored ADCP records have been shown to be effective in relating surface to subsurface flow structure, particularly in the internal wave band (Shay *et al.*, 1997, 1998) and to characterize near-surface shears (Shay *et al.*, 2002; Marmorino *et al.*, 2004). From the Duck94 data set, for example, Shay *et al.* (1998b) found 7 cm s^{-1} rms differences between the surface and subsurface currents acquired at 4 m beneath the surface from Vector Measuring Current Meters (VMCM). RMS differences of 10 to 16 cm s^{-1} between surface and VMCM moored up to 4 m beneath the surface were observed by Shay *et al.* (1995) and rms differences about 18 cm s^{-1} for a 15-m depth separation between surface and subsurface currents were reported for the same region (Shay *et al.*, 1998). Haus *et al.* (2000) reported good agreement between surface and subsurface velocities across the shelf, however at the inshore edge of the FC significant differences were found. Based on the previous studies with VHF mode in this region, there was good agreement between subsurface (3 and 4 m beneath the surface) and the surface current data. From the 4-Dimensional Ocean Current Experiment (1999), Shay *et al.* (2002) found differences from 13 to 22 cm s^{-1} for the velocity components between surface (OSCR) and subsurface currents measured at moorings and ship-board.

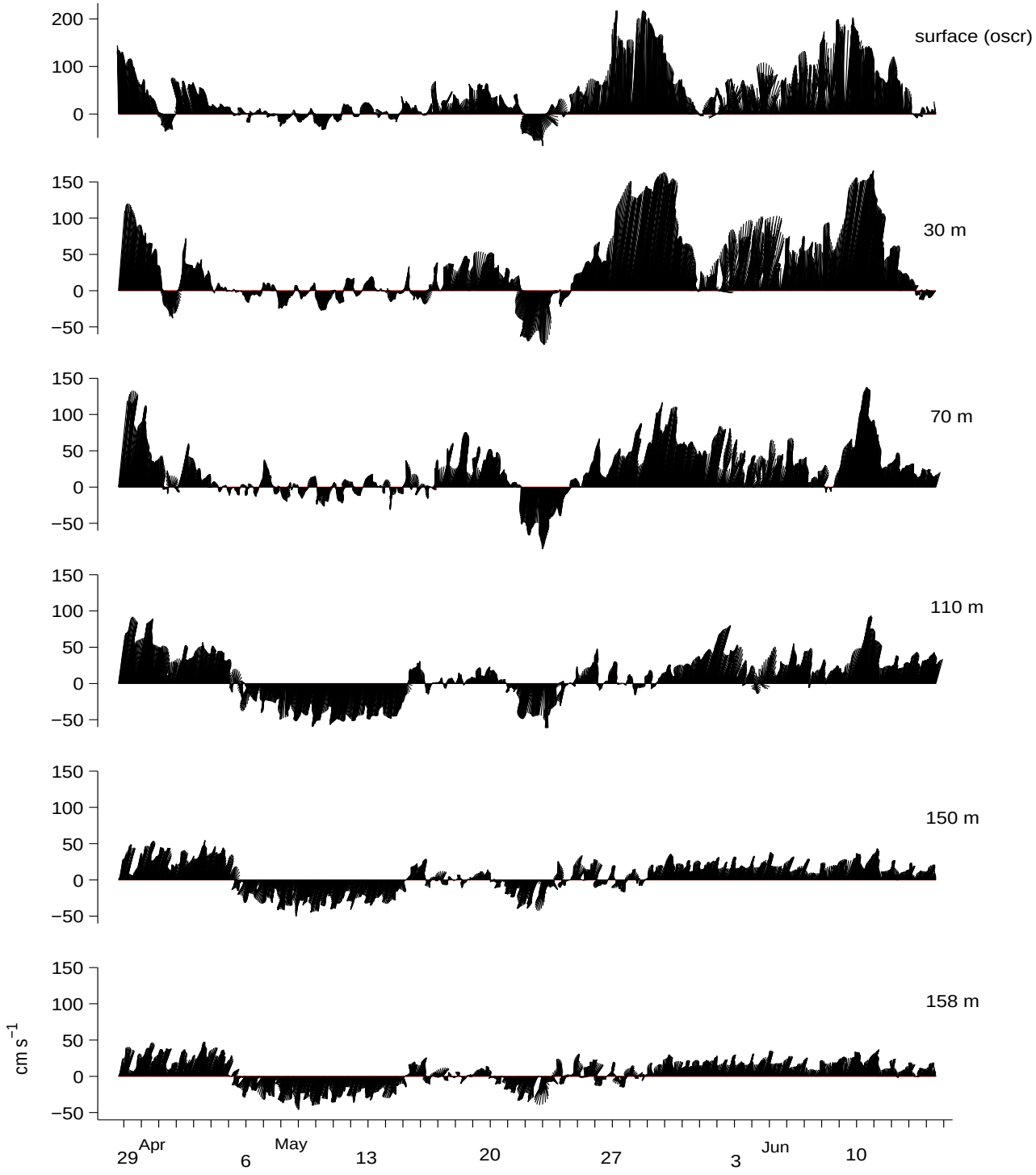

Figure 14: Vector plot of the time series of the surface currents at cell 473 and the ADCP-NSWC-A 165 m mooring at selected depths through the water column.

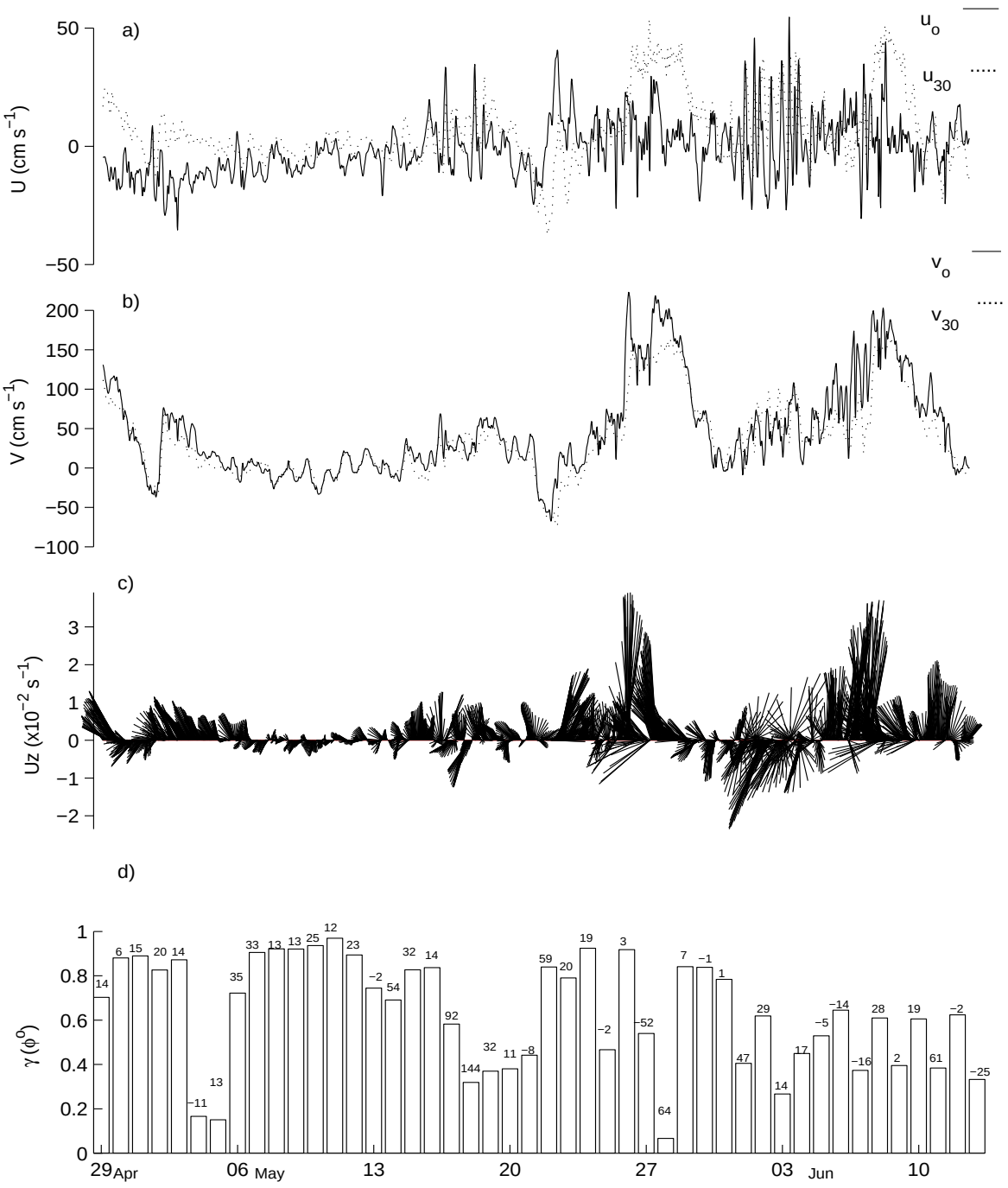

Figure 15: Observed time series at (NSWC-A) mooring from 29 April to 14 June 2001 for the surface (solid) and 30 m (dotted), (*a*) cross-shelf component (cm s^{-1}), (*b*) along-shelf component (cm s^{-1}), (*c*) bulk vertical shear ($\times 10^{-2}$ s^{-1}) over a 30-m layer and, (*d*) daily-averaged (72 points) complex correlation coefficients and phases listed above each bar.

Series	u_{o-b} cm s^{-1}	v_{o-b} cm s^{-1}	γ	ϕ ($\circ$)	$u_{o-b_{rms}}$ cm s^{-1}	$v_{o-b_{rms}}$ cm s^{-1}
$\vec{V_{30m}}$	-8	10	0.89	11.8	19	34
$\vec{V_{34m}}$	-11	13	0.88	14.4	18	36

Table 3: Averaged differences between the surface and subsurface currents for east-west (u_{o-b}) component, north-south (v_{o-b}) component, complex correlation coefficient (γ), complex phase angle (ϕ) and the *rms* differences in the east-west ($u_{o-b_{rms}}$) and north-south ($v_{o-b_{rms}}$) velocity components based on mooring data during NRL-2001 experiment.

Direct comparisons between surface currents over the upper 0.2 m and subsurface currents at 30-m depth from the ADCP indicated good agreement accounting for a 30-m depth separation between the two measurements. Cross-shelf surface currents were slightly weaker than 30-m subsurface currents (Figure 15), with an average flow of 9.6 cm s^{-1} at surface and 11.3 cm s^{-1} at 30-m depth. Surface currents in the along-shelf direction ranged between -60 to 220 cm s^{-1} and were at times larger than subsurface currents, particularly with the cross-shelf fluctuations of the FC. The corresponding along-shelf subsurface currents ranged between -70 to 165 cm s^{-1}. The complex correlation coefficient and phase angle (Kundu, 1976) are statistical measures of the relationship between the surface and subsurface current vectors. Daily-averaged (72 points) complex correlation coefficients indicated periods of high correlation ($\gamma > 0.8$) for 44% of the time series that included the event with weak oscillatory currents and FC reversals. During the last 18 days of the time series where large vertical shears occurred, the correlation coefficients were < 0.6. On 28 May, for example, the largest vertical shear occurred with $\gamma < 0.1$. On 4 to 5 May with the inshore edge of the FC farther offshore, correlations coefficients of 0.17 and 0.15 are apparent. Notice that the wind shift toward north on 18 May and toward northwest on 20 May caused a decorrelation ($\gamma < 0.4$) between surface and subsurface flows. The episodic nature of these large current shear events need to be further investigated in the region of submesoscale variability.

Surface and subsurface (30-m) current components were regressed on the basis of least squares fit (Figure 16). Mean biases between surface and 30-m depth data were 10.2 and -8.1 cm s^{-1} with slopes of 1.1 and 0.4 for the along and cross-shelf components respectively, which reflects the more energetic current variability in the along-shelf direction associated with the FC. The peak in the current differences was located at zero difference where the data followed a theoretical Gaussian distribution. RMS differences between surface and subsurface ranged from 18 to 36 cm s^{-1} for the velocity components, primarily due to the 30-m separation. A large fraction of these differences may be associated with the geophysical variability as suggested by Graber *et al.* (1997), internal waves (Shay *et al.*, 1997), and near-surface current shears associated with log layers (Shay *et al.*, 2002, 2003). Comparisons between subsurface currents at 30-m and 34-m were also made. RMS differences ranged from 2 to 3 cm s^{-1} for the velocity components, with a vertical shear of $\sim$0.5 to 0.8×10^{-2} s^{-1} over a 4-m layer, these results are also consistent with other studies (Shay *et al.*, 2003).

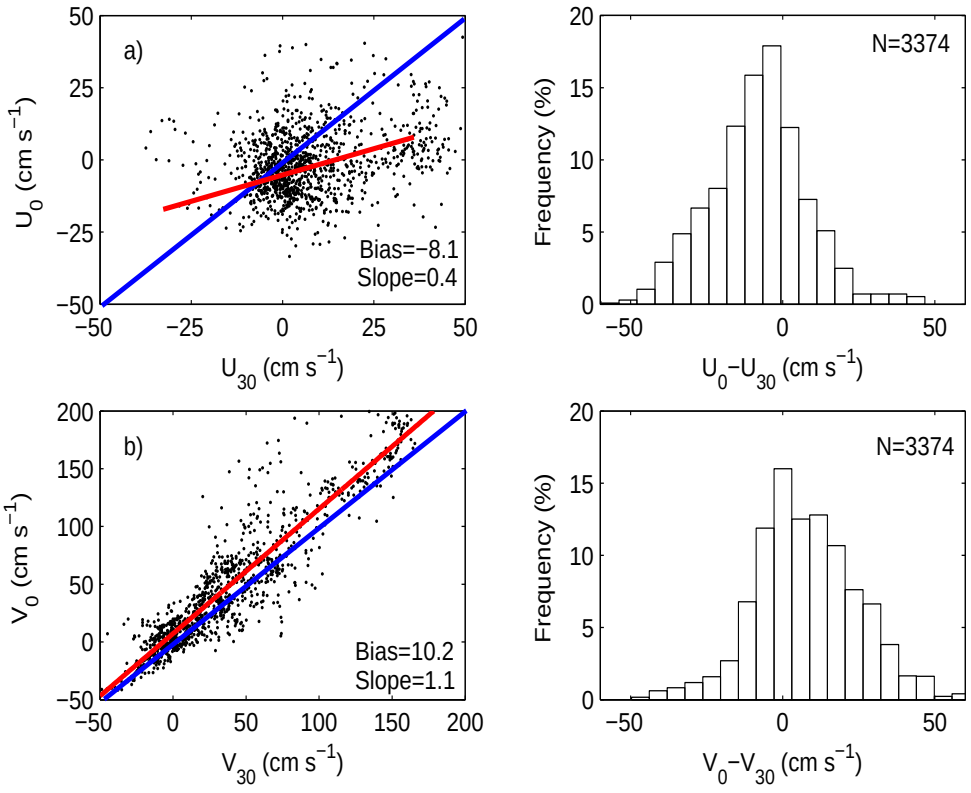

Figure 16: Scatter diagrams (left) with observed slope (red) and theoretical slope (blue), histograms (right) for the comparisons between surface and subsurface currents (30 m) at the ADCP (165 m) mooring, a) cross-shelf component, b) along-shelf component.

Profiler records from the ADCP were depth averaged from 30 to 158 m depth.

$$u_d = \frac{1}{H}\int_{-158m}^{-30m} u dz, \tag{13}$$

$$v_d = \frac{1}{H}\int_{-158m}^{-30m} v dz, \tag{14}$$

where H is the layer depth over 128 m. The depth-averaged currents were compared to the surface flows (Figure 17) to assess the importance of the baroclinic and barotropic processes contained within the surface currents. In the cross-shelf direction, both surface and depth-averaged component were weak (Figure 17a). Depth-averaged, along-shelf components were also weaker than the surface current (Figure 17b). Baroclinic currents were determined by removing the "depth-averaged flow" at the surface and 30 m (Figures 17c and 17d). Here the velocity components at each level revealed intermittent processes perhaps associated with baroclinic internal waves or other geophysical variability. For example, during one episode of mesoscale eddy, currents seemed to be predominantly barotropic (not shown) throughout the water column. This effect may appear to be barotropic when a deep baroclinic current such as the FC impinges across the shelf break, yet there will be significant current shears upon removal of the depth-dependent current.

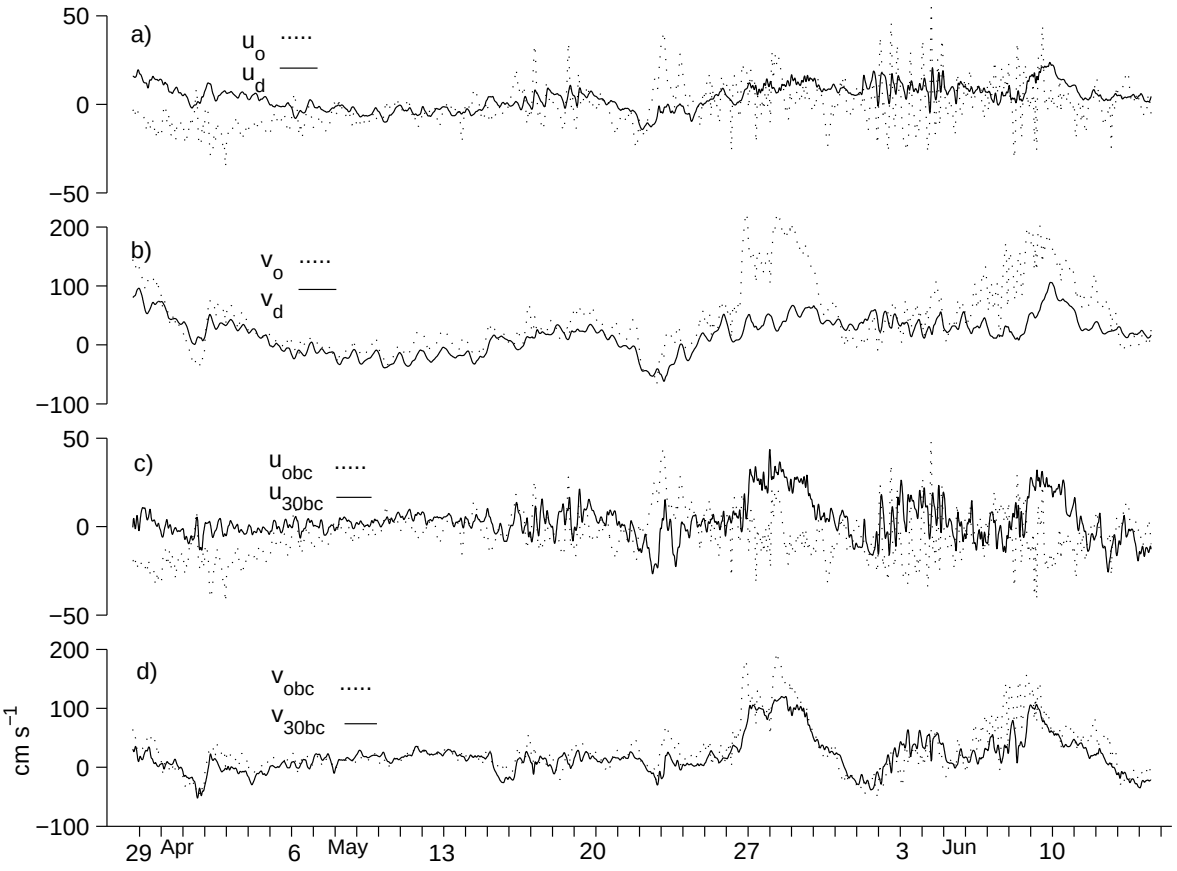

Figure 17: Comparisons of the surface(o), depth averaged (d), and baroclinic currents at the surface ($0bc$) and 30 m ($30bc$) for (a) u_0 (dash-dotted curve) and u_d (solid curve), (b) v_0 (dash-dotted curve) and v_d (solid curve),(c) u_{0bc} (dash-dotted curve) and u_{30bc} (solid curve) and, (d) v_{0bc} (dash-dotted curve) and v_{30bc} (solid curve).

4.5 Tidal Flows

The semidiurnal (M_2, L_2,S_2, N_2), diurnal (K_1, O_1, Q_1, J_1), and other higher-frequency (M_3, M_4, S_4) tidal constituents were isolated from the surface and subsurface currents time series at OSCR (cell 473) and the ADCP-NSWC-A at 30 m depth. Estimates of tidal currents were made using a harmonic analysis (Pawlowicz et al., 2002) with nodal corrections and confidence intervals computed for the analyzed components. As shown in Table 4, the dominant semidiurnal tidal components were the M_2 whereas the diurnal tides were O_1 and K_1 components. The variance explained by a linear combination of the 11 constituents ranged from 1 to 3% (Table 5) at this site with generally more in the east-west direction. In terms of variance, this equated to about 6 to 38 cm^2 s^{-2} with the larger values in the north-south direction. Tidal variability at 30 m depth was similar, where explained variances were 6 and 34 cm^2 s^{-2} in the cross-shelf and along-shelf direction, respectively.

The tidal time series, which are linear superposition of these constituents, indicated amplitudes of about ±5 to 7 cm s^{-1} in the cross-shelf direction, and ±8 to 12 cm s^{-1} in the along-shelf direction (Figures 18, 19). The analyzed non-tidal energy (not shown) is almost identical to the original time series for both components showing an insignificant amount of tidal energy. This is consistent with previous studies where tides generally explain only a few percent of the observed flows along the lower keys (see Shay et al., 1998b).

Var	Q_1	O_1	K_1	J_1	N_2	M_2	L_2	S_2	M_3	M_4	S_4	σ_o^2	σ_p^2	%
	cm s^{-1}											cm^2 s^{-2}		
u_o	1.4	0.7	0.8	1.4	0.0	1.5	0.8	1.7	1.0	0.8	0.7	191	6.9	3.6
ϕ_u	9	98	151	28	185	157	115	49	276	201	38			
u_{30}	1.0	1.8	1.3	1.0	0.9	0.8	0.8	1.0	0.3	1.2	0.3	226	5.8	2.6
ϕ_u	225	100	73	139	152	165	177	99	209	272	102			
v_o	1.0	5.0	5.7	1.5	0.3	2.6	1.6	1.4	1.5	0.1	0.7	3453	37.8	1.1
ϕ_v	349	32	355	333	304	329	244	2	334	209	14			
v_{30}	0.3	6.6	3.7	2.0	0.9	2.1	1.3	0.7	1.1	0.3	0.1	2432	34.0	1.4
ϕ_v	172	60	13	143	92	29	271	35	74	78	208			

Table 4: Tidal amplitude (u,v) and phase (ϕ_u,ϕ_v) of the 11 tidal components with 95% confidence interval estimates derived from a harmonic analysis of the cell-473 (u_0 and v_0) and NSWC mooring data at 30 m (u_{30} and v_{30}). Observed (σ_o^2) and predicted variance (σ_p^2) and the percent of explained variance by a summation of these tidal components are also given.

5 Summary

The coastal regime in the Florida Straits and the nearby coral reef tract along the Florida Keys is often subjected to energetic Florida Current fluctuations and the passage of storms. This westward boundary current represents a key part of the gyre circulation of the North Atlantic Ocean. Inshore of the current system, submesoscale variations are common where surface currents may be quite energetic, responding to both wind events as well these Florida Current intrusions. Under these physical forcing events, submesoscale vorticies, filaments and eddies are typically observed due in part to the large cyclonic current shears on the inshore side of the FC.

To observe the surface current manifestations of these ocean features, and their impact on the littoral zone, a shore-based phased array radar (OSCR) was deployed to measure currents. The NRL-2001 coastal field experiment was conducted in the South Florida in April-June 2001. The system operating in the Very High Frequency (VHF) band at 49.9 MHz mapped the surface currents vector field over a 7 km × 8 km domain with a horizontal resolution of 250 m at 700 grid points every 20 minutes. A total of 3374 samples were acquired yielding a fairly complete 47-day time series. Only 81 samples (2.4%) were missing from the vector time series, yielding one of the better OSCR deployments. Raw surface current vector data were transmitted to NRL each day

as part of their operations during the 47-day time series.

As suggested from previous studies, surface current measurements in the SFOMC revealed complex surface features, and were forced mainly by FC intrusions in the form of either horizontal wave-like meanders or the passage of submesoscale vortices. Surface currents were compared to subsurface measurements from moored Acoustic Doppler Current Profile (ADCP), and revealed biases of 8 to 10 cm s^{-1} and slopes of O(1) between surface and subsurface at 30 m beneath the ocean surface. RMS differences were about 18 to 34 cm s^{-1}, and bulk current shears were O(10^{-2} s^{-1}) in the FC where maximum velocities exceeded 2 m s^{-1} at the surface and 1.4 m s^{-1} between 30 and 50 m. Tidal currents were masked by the fluctuations of the Florida Current and were insignificant, explaining less than 4% of the current variance. Amplitudes of the dominant components were 2 to 7 cm s^{-1}, consistent with results from previous measurements.

To address these submesoscale variations, an HF-radar network for long-term monitoring of coastal and deep ocean ocean processes is being deployed along the East Florida Shelf (EFS) from Key Largo to Ft. Lauderdale. WEllen RAdar (WERA) sites will measure the surface current (and wave field) field based on beam-forming techniques from 16-element phased arrays at a frequency of 16 MHz with enough bandwidth to resolve currents at a spatial resolution of 750 m and an approximate range of about 100 km. The WERA system transmits a frequency modulated continuous wave (FMCW) chirp (0.26 sec) and avoids the 3 km blind range in front of the radar (Gurgel *et al.*, 1999; Essen *et al.*, 2000). For a transmission frequency of 16 MHz, the Bragg wavelength is 9.34 m and senses current over the top 75 cm of the water column (Stewart and Joy, 1974). The long-range version has been designed to acquire measurements to 100 km with a horizontal resolution of $\approx$ 750 m (bandwidth of about 200 KHz). Recent measurements along the West Florida Shelf (WFS) revealed periods of time when the range approached 120 km with the WERA system. RMS Differences between the surface and 4-m bin from an ADCP were about 6 cm s^{-1} along the 25-m isobath.

In support of the South East Atlantic Ocean Observing System along the EFS, this combination of high-temporal resolution over horizontal scales of less than 1 km from WERA will provide data to examine the relationship between submesoscale processes and their relationship to the large-scale FC where flows are predominately nonlinear and turbulent. Over the longer term, this approach will also raise more research questions about how the FC interacts with the coastal ocean circulation along the ecologically sensitive reef track of the Florida Keys. Clearly, such measurements will be of interest to a broad spectrum of groups working on scientific and management issues related to the coastal ocean.

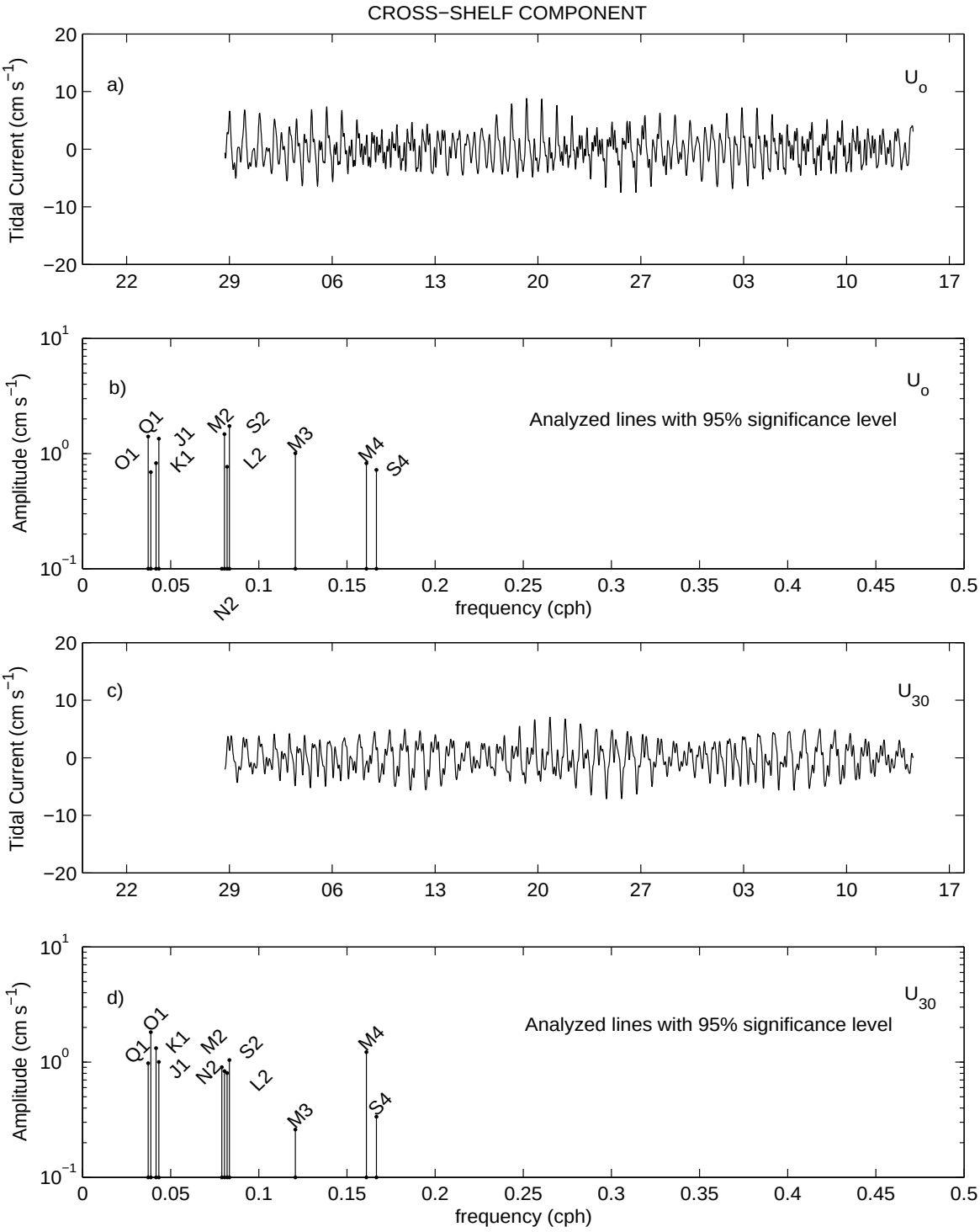

Figure 18: (*a*, *c*) Tidal time series using 11-tidal constituents for the cross-shelf currents at surface and 30 m. (*b*, *d*) Amplitude of all analyzed components with 95% significant level.

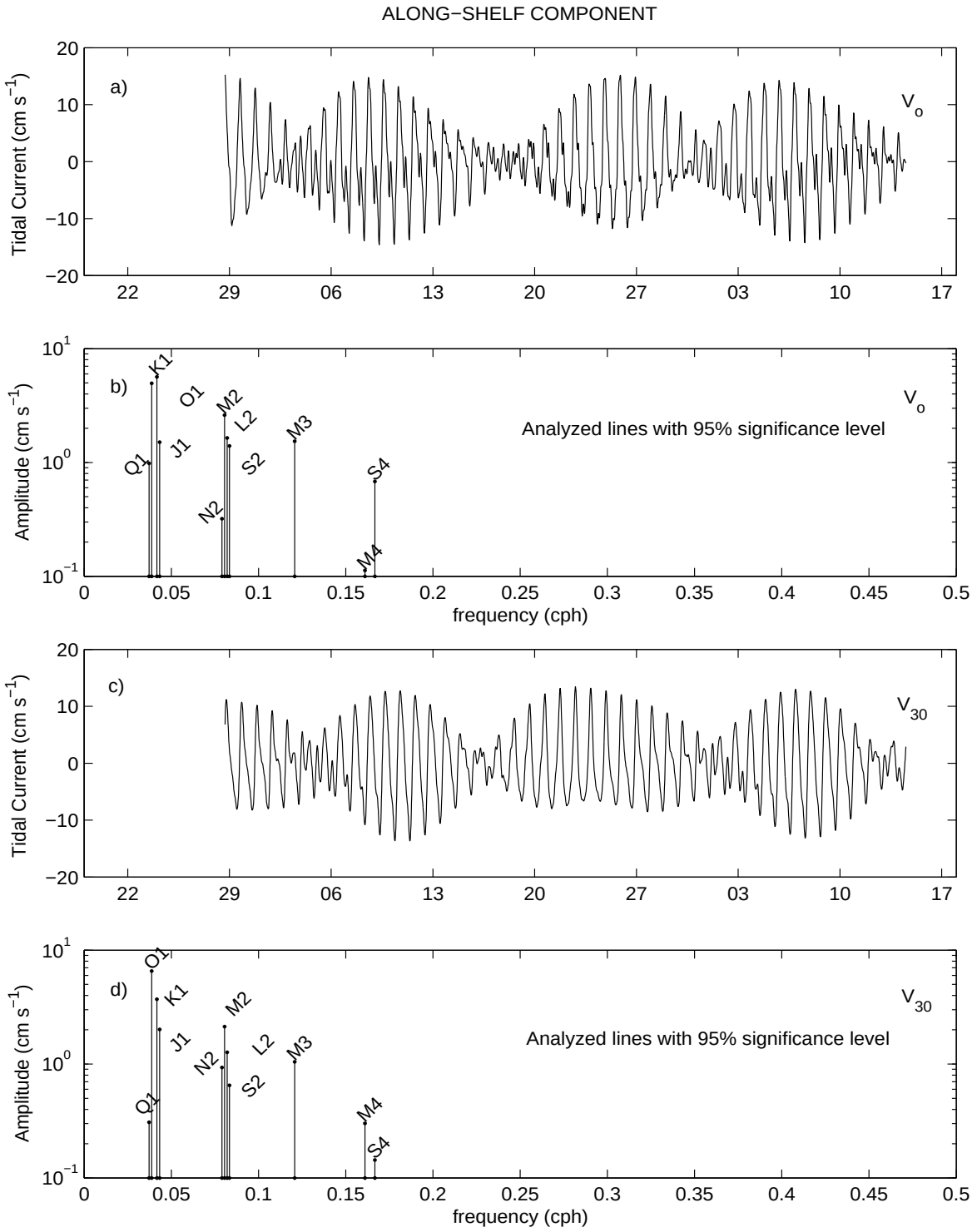

Figure 19: (*a*, *c*) Tidal time series using 11-tidal constituents for the along-shelf currents at surface and 30 m. (*b*, *d*) Amplitude of all analyzed components with 95% significant level.

6 References

Barrick, D. E., J. M. Headrick, R. W. Bogle, and D. D. Crombie, 1974: Sea backscatter at HF: Interpretation and utilization of the echo, *Proc. IEEE*, **62**, 673-680.

Crombie, D. D., 1955: Doppler spectrum of sea echo at 13.56 Mc s^{-1}, *Nature*, **175**, 681- 682.

Chapman, R. D., L. K. Shay, H. C. Graber, J. B. Edson, A. Karachintsev, C. L. Trump and D. B. Ross, 1997: On the accuracy of HF radar surface current measurements: Intercomparisons with ship-based sensors, *J. Geophys. Res.*, **102**, 18,737- 18,748.

Essen, H. H., K. W. Gurgel, and T. Schick, 2000: On the accuracy of current measurements by means of HF radar. *IEEE J. Oceanogr. Engin.*, **25(4)**, 472-480.

Graber, H. C., B. K. Haus, R. D. Chapman, and L. K. Shay, 1997: HF Radar comparisons with moored estimates of current speed and direction:expected differences and implications. *J. Geophys. Res.*, **102**, 18,749- 18,766.

Gurgel, K. W., G. Antonischki, H. H. Essen, and T. Schlick, 1999: Wellen Radar (WERA): a new ground wave HF radar for remote sensing, *Coastal Engineering*, **37**, 219-234, 1999.

Gurgel, K. W., H. H. Essen, and S. P. Kingsley, 1999: High frequency radars: limitations and recent developments, *Coastal Engineering*, **37**, 201- 218.

Haus, B. K., H. C. Graber, L. K. Shay, S. Nikolic, and J. Martinez, 1998: Ocean surface current obsevations with HF Doppler radar during the Chesapeake Outflow Plume Experiment (COPE-1). *RSMAS Tech. Report 98-003*, University of Miami. Miami, FL, 43 pp.

Haus, B. K., J. D. Wang, J. Rivera, J. Martinez-Pedraja, and N. Smith, 2000: Remote Radar Measurement of Shelf Currents off Key Largo, Florida, U.S.A. *Estuarine Coastal and Shelf Science*, Vol 51, **5**.

Kingsley, S. P., T. M. Blake, A. J. Fisher, L. J. Ledgard, and L. R. Wyatt, 1997: Dual HF radar measurement of sea waves from straight coastlines, Proceedings of 7^{th} International Conference on HF Radio Systems and Techniques, Nottingham. IEE, London, UK, July 1997.

Kundu, P. K., 1997: Ekman veering observed near the ocean bottom, *J. Phys. Oceanogr.*, **6**, 238-242, 1976.

Lee, T. N., 1975: Florida Current spin-off eddies, *Deep Sea Research*, **22**, 753-765.

Lee, T. N., D. A. Mayer, 1977: Low-frequency current variability and spin-off eddies along the shelf off Southeast Florida, *J. Marine Res.*, **35**(1), 193-220.

Marmorino, G. O., C. Y. Shen, T. E. Evans, G. J. Lindermann, Z. R. Hallock, and L. K. Shay, 2004: Use of 'velocity projection' to estimate the variation of sea-surface height from HF Doppler radar current measurements, *Continental Shelf Res.,*, **24**, 353-374.

Parr, A. E., 1937: Report on hydrographic observations at a series of anchor stations across the Straits of Florida, *Bull. of the Binghorn Oceanogr. Coll.*, **6**, 1-62.

Pawlowicz, R., R. Beardsley, and S. Lentz, 2002: Classical tidal harmonic analysis including error estimates in MATLAB using T-TIDE, *Computers & Geosciences*, **28**, 929- 937.

Peters, H., L. K. Shay, A. J. Mariano, and T. M. Cook, 2002: Current variability on a narrow shelf with large ambient vorticity, *J. Geophys. Res.*, **107**(C8).

Peters, N. J., and R. A. Skop, 1997: Measurements of ocean surface currents from a moving ship using VHF radar, *J. Atmos. Oceanic Technol.*, **14**, 676-694.

Prandle, D., 1987: The fine-structure of nearshore tidal and residual circulations revealed by HF radar surface current measurements. *J. Phys. Oceanogr.*, **17**, 231-245.

Shay, L. K., 1997: Internal waves detected by HF radar, *The Oceanogr. Soc.*, **10**(2), 60-63.

Shay, L. K., H. C. Graber, D. B. Ross, and R. D. Chapman, 1995: Mesoscale ocean current structure detected by high-frequency radar, *J. Atmos. Oceanic Technol.*, **12**, 881-900.

Shay, L. K., T. N. Lee, E. J. Williams, H. C. Graber, and C. G. H. Rooth, 1998: Effects of low frequency current variability on near- inertial submesoscale vortices, *J. Geophys. Res.*, **103**(C9) , 18, 691-714.

Shay, L. K., S. J. Lentz, H. C. Graber, and B. K. Haus, 1998b: Current structure variations detected by high frequency radar and vector measuring current meters, *J. Atmos. Oceanic Technol.*, **15**, 237-256.

Shay, L. K., T. M. Cook, B. K. Haus, J. Martinez, H. Peters, A. J. Mariano, P. E. An, S. Smith, A. Soloviev, R. Weisberg, and M. Luther, 2000: VHF radar detect oceanic submesoscale vortex along Florida coast, *EOS*, **81**(19), 209, 213.

Shay, L. K., T. M. Cook, H. Peters, A. J. Mariano, R. Weisberg, P. E. An, A. Soloviev, and M. Luther, 2002: Very high frequency radar mapping of surface currents, *IEEE J. of Oceanic Engin.*, **27**, 155-169.

Shay, L. K., T. M. Cook, and P. E. An, 2003: Submesoscale coastal ocean flows detected by very high frequency radar and autonomous underwater vehicles. *J. Atmos. Oceanic Technol.*, **20**, 1583-1599.

Stewart, R. H., and J. W. Joy, 1974: HF radio measurements of surface currents, *Deep Sea Res.*, **21**, 1039-1049.